Provided for non-commercial research and education use.
Not for reproduction, distribution or commercial use.

Volume 33 Number 3 March 2008 ISSN 0960-1481

ELSEVIER

Renewable Energy
AN INTERNATIONAL JOURNAL

Editor-in-Chief: A.A.M. Sayigh

This article was published in an Elsevier journal. The attached copy is furnished to the author for non-commercial research and education use, including for instruction at the author's institution, sharing with colleagues and providing to institution administration.

Other uses, including reproduction and distribution, or selling or licensing copies, or posting to personal, institutional or third party websites are prohibited.

In most cases authors are permitted to post their version of the article (e.g. in Word or Tex form) to their personal website or institutional repository. Authors requiring further information regarding Elsevier's archiving and manuscript policies are encouraged to visit:

http://www.elsevier.com/copyright

Author's personal copy

Available online at www.sciencedirect.com
ScienceDirect
Renewable Energy 33 (2008) 520–529
RENEWABLE ENERGY
www.elsevier.com/locate/renene

Technical Note

A novel direct-drive ocean wave energy extraction concept with contact-less force transmission system

Emmanuel B. Agamloh*,[1], Alan K. Wallace, Annette von Jouanne

School of Electrical Engineering and Computer Science, Oregon State University, Corvallis, OR 97331, USA

Received 2 March 2006; accepted 22 January 2007
Available online 26 March 2007

Abstract

This paper describes the design and testing of a new rotary direct-drive ocean wave energy extraction system. The device employs a contact-less force transmission system (CFTS) to couple a float to the power take-off (PTO) mechanism made up of a ball screw, unidirectional clutch and a permanent magnet generator. Comprehensive simulation, design and testing of both the force transmission system and the ocean energy extraction system are presented along with preliminary wave flume test results of the buoy in irregular waves.
© 2007 Elsevier Ltd. All rights reserved.

Keywords: Contact-less force transmission system; Ocean wave energy

1. Introduction

The commonly proposed ocean energy extraction techniques are based on hydraulic or pneumatic intermediaries that are prone to failures, with high maintenance costs. One way of eliminating the intermediate systems is to use direct-drive techniques to convert the slow linear motion, produced by the waves, to rotary or linear motion by means of an efficient and simple system. The authors have recently proposed a novel direct-drive linear generator [1]. The current rotary direct-drive approach requires innovative systems not only for efficient conversion of the slow motion of waves into high rotary speeds for power take-off (PTO) systems, but also as an effective means of transmitting the force from the ocean waves onto the PTO mechanisms. In the severe ocean environment, the PTO components must be sealed from exposure. In addition, the wave excitation forces, developed by devices such as buoys, have to be transmitted to those sealed components. In this paper, a contact-less force transmission system (CFTS) is proposed, which employs magnetic fields for contact-less mechanical thrust transmission. This system has enhanced the design of a new direct-drive ocean wave energy converter (OWEC) using a ball screw to act as a mechanical gear system for fast speed and torque transmission.

Ball screws have been used for many years in machine building and are often a key mechanical component in machines that rely upon rotary/linear motion conversion, e.g. lathe machines. Many other machines that use ball screws can be found in industrial plants and mechanical workshops. Over the years, ball screws have proved to be a reliable component in machines and are still widely used. Many machines equipped with ball screws operate in manufacturing plants on a continuous basis. The authors are of the opinion that this reliability feature could be an important benefit in a wave energy device.

The term "direct" drive describes the direct coupling of the buoy's velocity and force to the generator without the use of hydraulic fluid or air. Generators that are designed to operate with the low speeds of wave excitation are often referred to as direct drive [1,2]. In this device, a ball screw

*Corresponding author. Tel: +1 541 737 0831; fax: +1 541 737 1300.
E-mail addresses: eagamloh@advancedenergy.org (E.B. Agamloh), wallace@eecs.oregonstate.edu (A.K. Wallace), avj@eecs.oregonstate.edu (A. von Jouanne).
[1]Currently with Advanced Energy Corporation, Raleigh, NC 27606.

0960-1481/$ - see front matter © 2007 Elsevier Ltd. All rights reserved.
doi:10.1016/j.renene.2007.01.008

Author's personal copy

Nomenclature

n_s	synchronous speed of generator
a	buoy added mass
b_1	hydrodynamic damping
b_G	generator damping coefficient
E	electromotive force
I_{MG}	moment of inertia
T_{screw}	ball screw torque
F_{screw}	ball screw thrust
F	wave excitation force
Ω	shaft angular speed of rotation
l	ball screw lead
L_j	generator phase inductance
K_T	generator breaking torque constant
K_f	emf constant of generator

shaft is used to couple the generator, and the "direct" drive term is applied here to maintain the distinction between devices that rely on hydraulic and pneumatic intermediate systems for operation and those that do not.

The CFTS has been modeled and optimized using finite element analysis (FEA) and the results have been validated with experimental testing. Also, the device has been modeled in Matlab/Simulink using linear wave theory. Finally, preliminary results from wave flume testing have also been presented.

2. Description of the overall system

The solid model of the overall buoy system is shown in Fig. 1 with components such as the CFTS, ball screw and ball nuts displayed in the section view. The system comprises an outer float inside which is a ferromagnetic cylinder which slides against an inner module that contains the PTO components. As the outer float slides, it pulls the piston of the inner module along, with the help of the CFTS. The inner module is completely sealed. The buoyancy force on the outer cylinder is transmitted through the wall of the inner module to the ball nut by the magnetic fields of the piston.

Fig. 2 shows the actual realization of the overall buoy system displayed in the Motor Systems Resource Facility (MSRF) main testing laboratory. The actual implementation includes an aluminum base plate with three studs on which weights are placed to hold down the buoy during operation. The actual implementation also has the generator located on top of the inner module but it could, in fact, be located at the base of the inner module without any change in performance.

The overall dimension of the outer float is 0.6 m diameter and 0.6 m length. The inner module is about 1.7 m and its active length, as determined by the screw shaft length, is about 1 m. The outer buoy was made from a PVC barrel and covered with top and bottom plates made of PVC. The

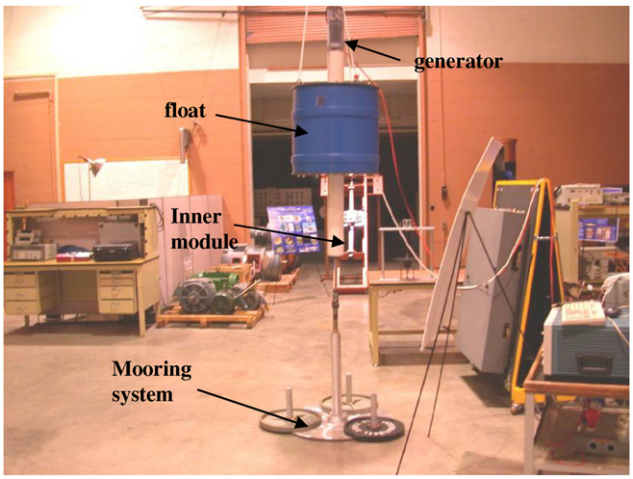

Fig. 2. Actual implementation of buoy system.

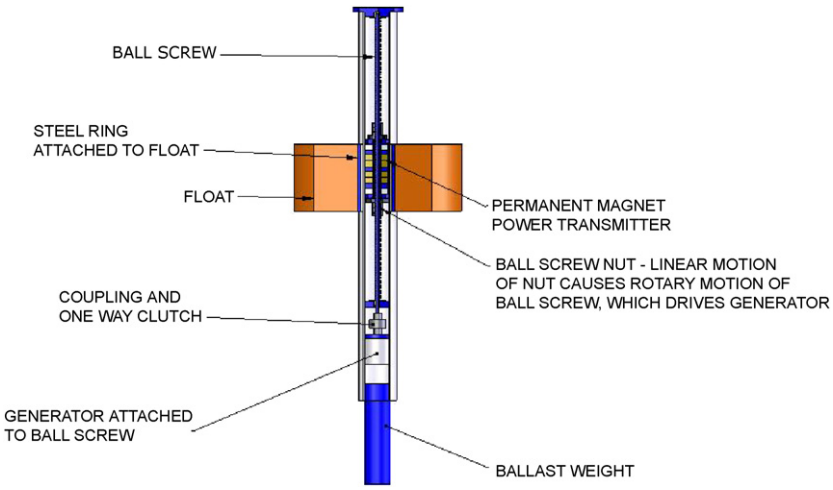

Fig. 1. Solid model of buoy system.

Author's personal copy

float also contains the back-iron cylinder enclosed in a machined PVC housing. The inner module is made of PVC tube and machined end caps.

3. The CFTS

3.1. Description

The CFTS is a tubular ferromagnetic reluctance device of two components. The first component consists of neodymium–iron–boron (NdFeB) magnets which are axially magnetized and configured in a "piston" with two opposing poles squeezing magnetic flux radially through a central pole piece into the back-iron "cylinder" (the second component) which is mounted on the buoy. The reluctance force that is developed when the buoy moves up and down is transmitted to the piston through the magnetic field between these two components. The motion of the piston is then transformed to rotation using a roller/ball screw to drive a permanent magnet rotary generator. The entire permanent-magnet piston/ball-screw/generator system is completely sealed and enclosed. As there is no physical contact between the piston and the cylinder, the system will not be damaged if subjected to overloads (such as in storm conditions). It is expected that under such extreme conditions, the system will "slip" and recover when normal sea conditions are restored. When slip occurs, the salient steel back-iron is no longer under the influence of the magnetic field and is only under the influence of the wave conditions. Since there are no electrically conducting materials in the force transmission system, heating effects would not be an issue.

3.2. Design of the CFTS

The CFTS develops reluctance force between the salient cylinder back-iron and the permanent magnets on the piston. The arrangement of the magnetic system of the force transmission system is similar to the transverse flux machine, the tubular linear generator or the switched reluctance motor. Previous researchers have found that for optimal design of these machines, certain parameters, including the pole pitch to air gap ratio, and the tooth width to pole pitch ratio lie within specific ranges [2–5].

In this application, some of the parameters have significant mechanical and structural implications. For example, although a smaller air gap may be desirable to develop high thrust or torque in these machines, the air gap of the CFTS is essentially determined by the thickness of the inner module as well as clearances for easy reciprocal movement. The thickness of the inner module cylinder must be chosen to prevent it from flexing, which can cause obstruction. Also, the diameter of the inner module depends on the magnet arrangement used on the piston. On the other hand, in the machines mentioned above, the air gap thickness is dictated largely by mechanical clearance. Although the effects of electrical loading and armature reaction are not relevant in this application, the methods reported in [2–5] would enhance further investigation of the CFTS in its future improvements, with respect to optimal design of the back-iron and the permanent magnet system.

Refs.[6,7] also present analytical expressions for the computation of forces of interaction in permanent magnet couplings with both inner and outer magnets. Due to symmetry and ease of modeling the system, finite element simulations have been used in this work to simplify the design process.

The design of the force transmission system progressed through three prototype stages. A number of configurations of permanent magnet arrangement and design of the back-iron cylinder were investigated for optimum transmission of thrust as shown in Fig. 3. All constructions used ring-type magnets and ring-shaped soft iron pole pieces on the piston and cylindrical back-iron. The salient constructions (Designs #2, #3, #4) were better than the non-salient construction (Design #1). Also, the thrust characteristics of Designs #2 and #3 were not significantly different.

The final design of the piston that was adopted for the device has four ring-type magnets of the following dimensions: external diameter—100 mm, internal diameter—50 mm, axial thickness—25 mm. The magnets were stacked up in pairs per pole piece and interspersed with soft iron ring-shaped pole pieces 10 mm thick. This piston was

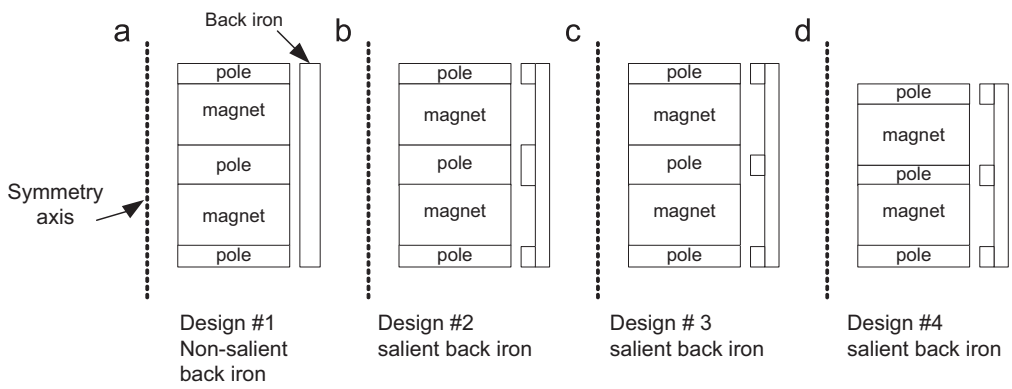

Fig. 3. Design configurations of CFTS.

Author's personal copy

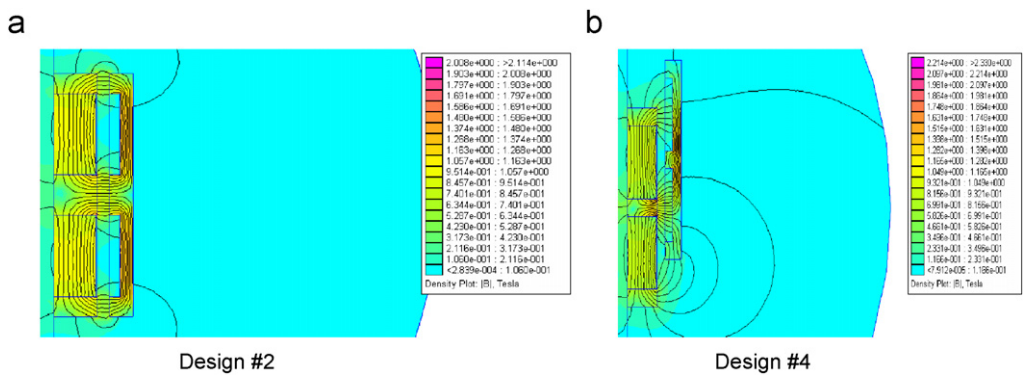

Fig. 4. 2D finite element modeling.

configured in Design #4 arrangement and it produced a peak axial thrust of about 900 N. By comparison, a smaller version of the piston in Design #1 configuration and with smaller magnets of external diameter—55 mm, internal diameter—25 mm, axial thickness—20 mm and about 10-mm-thick pole pieces produced a peak axial thrust of about 120 N. The peak thrust increases dramatically with the increase in volume of the piston in general and, in particular, the size of the magnets as well as saliency of the back-iron, as subsequent results would show.

3.3. FEA of the CFTS

FEA was employed to investigate alternative Designs #2 and #4 as shown in Fig. 4 using software developed by [8]. The main difference between these two configurations is the size of the central pole piece. In Design #2, the central pole piece is twice the size of the outer pole pieces. In a conventional tubular machine, this would have been the arrangement of pole pieces to create a symmetrical system of equal flux linkage to all phases in order to produce balanced two or three phase voltages. As there are no such requirements in this application, Design #4, which has all pole pieces of the same size, is also possible and has been investigated. It turned out that this design had the highest peak axial thrust as discussed subsequently.

The results of computed force capability as functions of piston–cylinder displacement are given in Fig. 5. As shown in the FEA results in Fig. 5, the peak thrust of Design #4 is higher than that of Design #2. The peak thrust is obtained at a displacement approximately equal to one pole dimension. However, the thrust characteristics of Design #2 are wider than that of Design #4, with high thrusts distributed over a wider range of axial displacement.

The difference in the two characteristics is interesting and can be attributed to saturation of the central pole in Design #4 compared to Design #2 and the effects of flux leakage. In Design #4, the effects of saturation of the central pole make the thrust lower compared to Design #2 at higher displacements. On the other hand, the large central pole piece and consequently larger dimensions in Design #2 allow for increased leakage, which generally

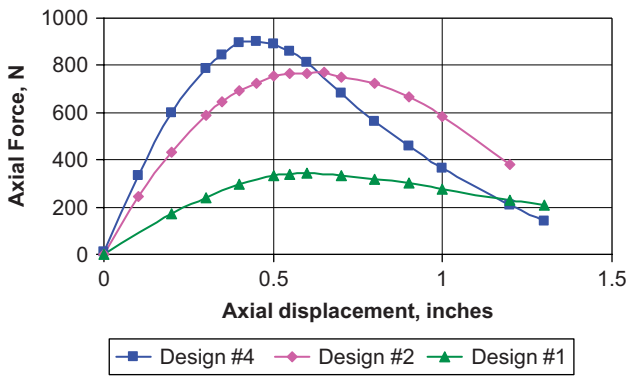

Fig. 5. 2D finite element modeling, axis symmetric computation of thrust.

Table 1
Comparison of finite element data for piston/cylinder configurations for 3/4 shaft CFTS

Design configuration	Peak thrust (N)	Remarks
Design #1	343	Non-salient back iron
Design #2	763	Salient back iron type1
Design #3	769	Salient back iron type2
Design #4	900	Salient back iron type3

reduces the flux density and thrust. Depending on the required application, either curve can be chosen either to maximize the peak thrust (Design #4) or to allow adequate vertical travel (Design #2). The peak thrusts of all the configurations are compared in Table 1.

The FEA results were validated with experimental testing to determine the peak output thrust for two different prototypes, implemented with different shaft sizes as shown in Table 2. There was a strong agreement between the FEA results and the test results.

3.4. Laboratory testing of the CFTS

The laboratory testing of the CFTS was carried out in the MSRF by applying known thrust to the cylinder and

Author's personal copy

measuring the electrical output of the permanent magnet generator coupled to the shaft. Two permanent magnet generators, as shown in Fig. 6, were investigated for this project. Both of them operated differently when coupled to the same shaft and loaded under similar conditions due to significant differences in their impedances. This indicates that not only the power rating, but also, the characteristics of the generator for this application must be carefully considered at the design stage.

Generator #1 was the generator intended for use in the buoy. However, in order to increase the travel of the outer float, it was thought that the generator that would be used should fit into the inner module so that the outer float would be able to slide past it. Generator #2 fits well into the inner module and was used for the wave tank testing, though its impedance was very high and there was significant voltage drop across its windings when it was loaded.

The laboratory setup for the testing is shown in Fig. 7. A known thrust is obtained by attaching weights to the outer cylinder and releasing it to accelerate under gravity. The speed measurement was obtained from the oscilloscope capture of the output waveform by measuring its frequency and using the equation for the speed of a synchronous generator

$$n_s = \frac{120f}{p}, \tag{1}$$

where p is the number of poles and f is the frequency. From the calculated speed, the axial velocity is obtained from the formula $\Omega = dz/dt(2\pi/l)$ [rad/s], using the screw lead, where Ω is the mechanical speed of rotation of the shaft. The input power to the system is the product of the applied thrust and linear velocity and the output power is measured directly as the electrical power dissipated in the resistances that were connected across the generator. Possible experimental errors in the measurements were minimized by using precision weights, that are normally used for calibration purposes, to generate the thrust. Also a high-end Tektronix digital phosphor oscilloscope was used for

Table 2
Validation of peak axial thrust from finite element modeling and experimental test

Prototype	FEA model prediction	Test
Peak axial force (N)		
3/8 Shaft	122	117.6
3/4 Shaft	900	894.3

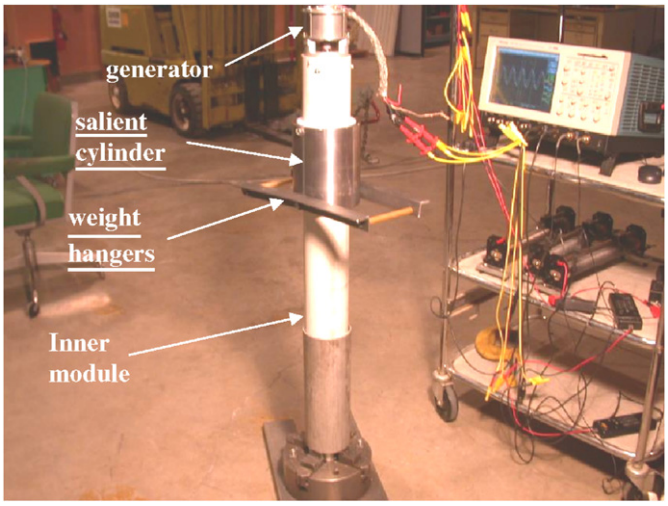

Fig. 7. CFTS, measurement of conversion efficiency.

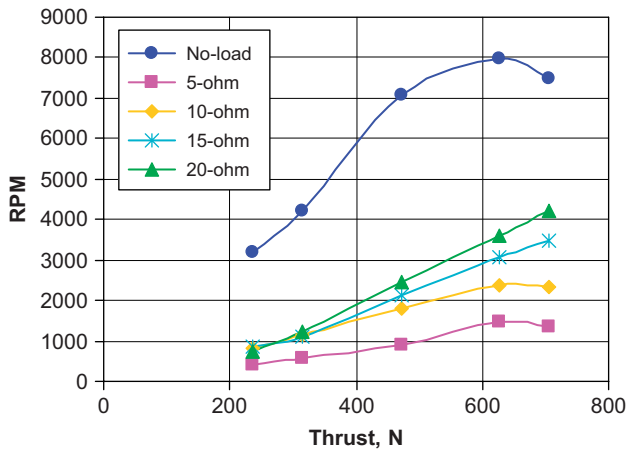

Fig. 8. Generator shaft speed under load and during no load operation.

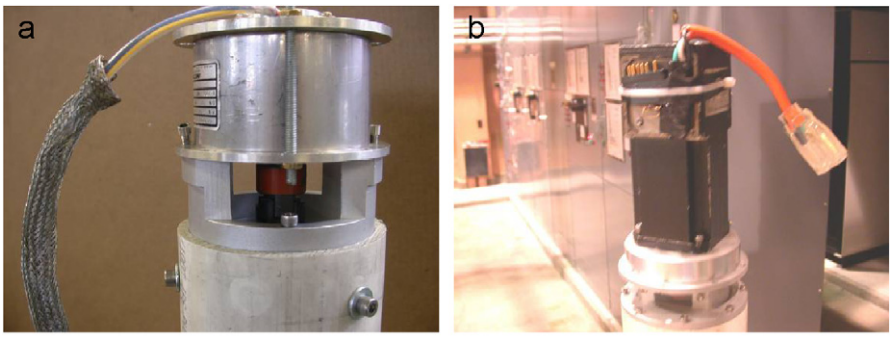

Generator #1 Generator #2

Fig. 6. Permanent magnet generators.

Author's personal copy

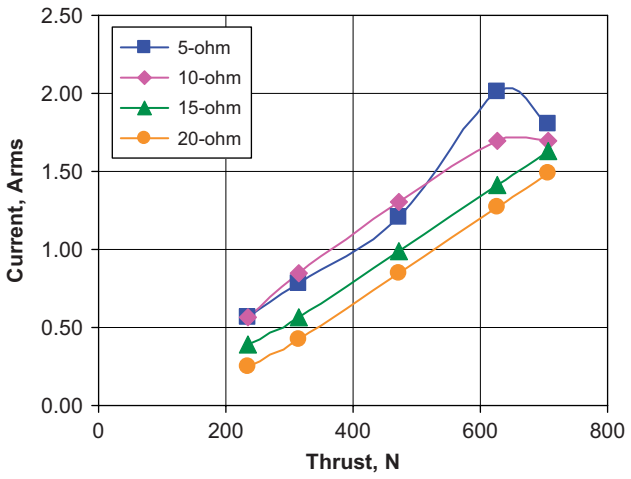

Fig. 9. Generator load current.

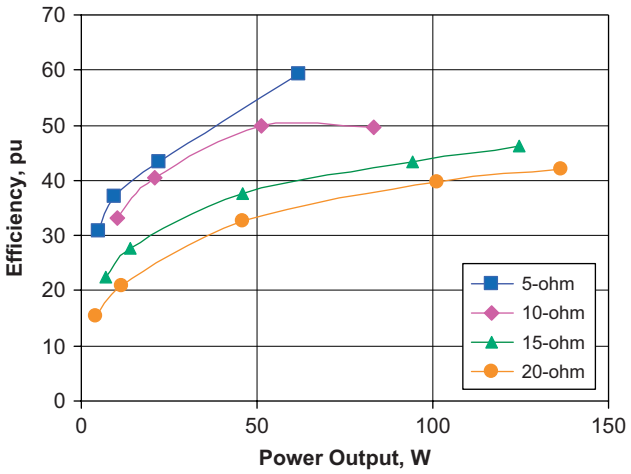

Fig. 10. System efficiency.

measurement of frequency and the voltage and current signals as shown in Fig. 7.

Figs. 8–10 show the test result of generator #1 during the laboratory testing to determine the system efficiency. Fig. 8 shows the shaft speed of the generator under load and during no load operation. Under no-load, the higher speeds result in higher frictional losses and consequently a non-linear speed-thrust characteristic. Under load, the generator speed is much lower and is more linear with thrust. The current, as expected, increases fairly linearly with the applied thrust as shown in Fig. 9. The overall system efficiency is greater than 50% for the 10 Ω load but falls as the electrical load is reduced. Similar curves were obtained for generator #2, except that its high impedance resulted in significant voltage drops and lower power output.

4. Simulation of the OWEC using Matlab/Simulink

The equation of motion of the device, in a single degree of freedom heave mode, is given by [9–11]

$$m_v\ddot{z} + b\dot{z} + cz = F_0\cos(\omega t + \sigma), \tag{2}$$

where $m_v = (m+a)$ is the total virtual mass of the buoy including the added mass a, b is the damping of the buoy comprising the hydrodynamic damping of the waves (b_1) and that provided by the PTO generator (b_G), c is the spring (buoyancy) constant, $F = F_0\cos(\omega t+\sigma)$ is the exciting force from the waves and $z = z_0\cos(\omega t)$ is the heave displacement. The added mass a, hydrodynamic damping b_1 and the spring constant c are given by McCormick [9] for a cylindrical buoy.

The damping constant of the generator is determined from the following considerations. A ball screw comprises a shaft with inclined threaded groove and a nut that is concentric to the shaft. The nut also contains small cylindrical steel balls that pass through the grooves (see Fig. 11). Traditionally, ball screws are used to convert rotational motion to linear motion. By spinning the shaft in any given direction, the nut moves linearly up or down the length of the shaft, thus converting rotary to linear motion in a process called forward driving.

Alternatively, as the nut is pulled up or down, the shaft rotates in the clockwise or counterclockwise direction, respectively, thus converting linear to rotary motion. This process is known as back driving and is employed in this application. The force that is applied to move the nut up and down is derived from the waves through the CFTS described in Section 3.

The relationship between the torque on the shaft T_{screw} and the axial force F_{screw} for the ball screw is given by

$$T_{screw} = \frac{lF_{screw}}{2\pi\eta_f} \quad \text{(forward driving)}, \tag{3a}$$

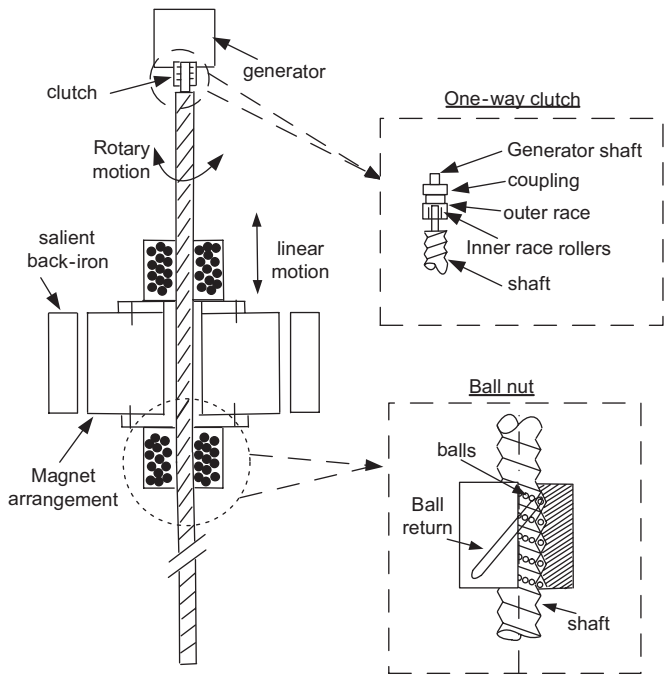

Fig. 11. Details of ball screw mechanism.

Author's personal copy

$$T_{\text{screw}} = \frac{lF_{\text{screw}}}{2\pi}\eta_{\text{b}} \quad \text{(back driving)}, \tag{3b}$$

where l is screw lead [m/rev], and η_{f}, η_{b} are the forward and back drive efficiencies of the ball screw, respectively. The generator basically acts as a brake, opposing the rotation with a torque on the shaft that can be expressed as

$$T_{\text{screw}} = K_{\text{T}}\Omega + T_0, \tag{4}$$

where T_0 is loss torque [Nm], K_{T} is braking coefficient of the generator [Nms/rad] and Ω is angular velocity of the shaft. For instance, if a permanent magnet synchronous generator (PMSG) is used, as in this project, the introduction of the constant K_{T} effectively assumes a linear magnetic circuit with no saturation of the rotor and stator iron. With the relatively large effective air gaps (of the magnets themselves) that are common in permanent magnet generators, this assumption would not lead to significant errors.

The total PTO force during the upstroke is then given by

$$F_{\text{screw}} = \frac{2\pi}{l}(K_{\text{T}}\Omega + T_0 + I_{m\text{G}}\alpha), \tag{5}$$

where I_{mG} is the moment of inertia of the generator and shaft system, and for the roller screw $\Omega = \dot{z}(2\pi/l)$, where $\dot{z}$ is linear velocity of the ball nut or similarly velocity of the float, and $\alpha = \mathrm{d}\Omega/\mathrm{d}t = \ddot{z}(2\pi/l)$ is the angular acceleration of shaft. The generator damping coefficient is given by

$$b_{\text{G}} = K_{\text{T}}\left(\frac{2\pi}{l}\right)^2. \tag{6}$$

Because the generator is decoupled, during the down stroke, there is no axial force from the PTO on the buoy. The generator "free wheels", i.e. it is decelerated by the electrical load connected to it, its own inertia and that of the shaft through the unidirectional clutch. We then have $F_{\text{screw}} = 0$ or

$$I_{\text{mG}}\alpha + T_{\text{screw}} = 0. \tag{7}$$

The unidirectional clutch allows torque to be transmitted in only one direction. The clutch comprises two main parts: the inner race and the outer races with several sprags or rollers and springs embedded between the inner and outer races. The clutch operation is similar to the ratchet wrench, a commonly used mechanical tool, in which operation in one direction locks up the inner and outer races to transmit the required torque while operation in the other direction overruns or "free wheels". In this device, the outer race is connected to the generator coupling and the inner race is connected to the screw shaft.

The use of a unidirectional clutch enables operation of the generator in only one direction, although the generator is capable of operation in both directions. Due to the need to rectify the intermittent output of the generator, both unidirectional and bidirectional operation is possible. However, it is important to note that, unlike in direct drive linear generators where low speeds are used for driving the generator, the rotary device operates at high speeds and reversing the generator would cause additional mechanical stresses in the rotating mechanisms.

On the other hand, during unidirectional operation, the rotating inertia on the upstroke can be utilized when the generator is not fully decelerated on the downstroke before the next upstroke begins.

The equivalent circuit of the permanent magnet synchronous generator is shown in Fig. 12. The voltage across a phase of the generator windings can be expressed as

$$v_j = -r_j i_j + L_j\frac{\mathrm{d}i_j}{\mathrm{d}t} + \frac{\mathrm{d}\lambda_{j\text{f}}}{\mathrm{d}t}, \tag{8}$$

where r_j is phase resistance, i_j is current of the j-th phase, $\lambda_{i\text{f}}$ is flux linkage in phase j due to the permanent magnet and L_j is phase inductance.

The peak value of the induced emf of the PMSG is dependent on speed and can be expressed as $E_j = \mathrm{d}\lambda_{i\text{f}}/\mathrm{d}t = K_{\text{f}}\Omega$. The currents can be obtained by rearrangement and integration of Eq. (8), noting that $v_1 = i_1 R_{\text{load}}$. The generator parameters were determined from test measurements and are given in Appendix A.1.

The no-load voltage of the generator during operation in waves with a unidirectional clutch action on the shaft under the wave conditions of $T = 2.5$ and $H_{\text{s}} = 0.15\,\text{m}$ is given in Fig. 13. During free wheeling, the voltage produced is zero as the clutch disengages the generator from the rotation and the generator is decelerated. Also,

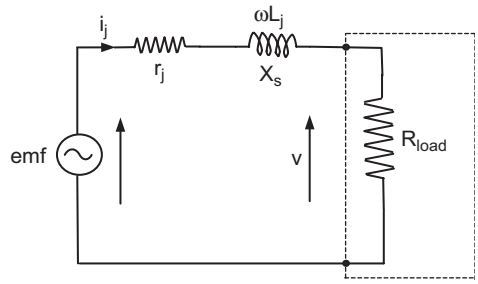

Fig. 12. Equivalent circuit for the PMSG.

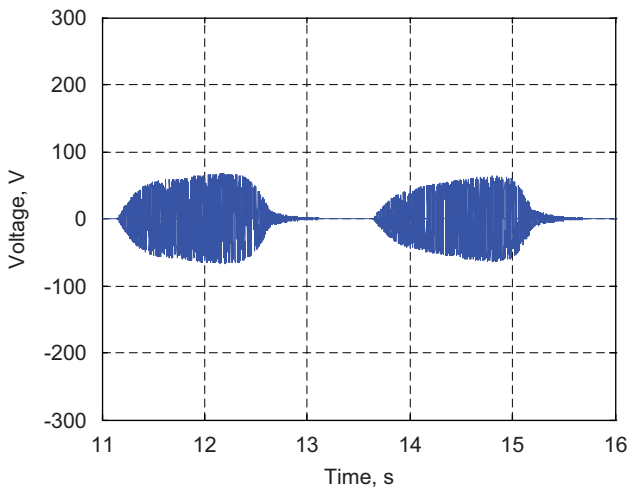

Fig. 13. Typical no-load voltage of CFTS buoy with clutch.

Author's personal copy

unlike operation under the reciprocating action, with a clutch the voltage time area is less symmetrical. This is similar to results obtained during experimental testing in waves.

The results obtained from Matlab simulation strongly correlate to the experimental testing results as shown in Figs. 13 and 15. The Matlab analytical model can therefore be used for the investigation of pertinent design parameters during the conceptual design phase. One such parameter is the pitch or the lead of the ball screw. A screw with a small screw lead allows for high speeds but has a lower torque capability and vice versa. Since the main benefit of the rotary system is to utilize the high-speed capability of rotary generators, it is important to understand the effects of various screw leads on the performance, and analytical modeling is useful for these investigations. Also, the Matlab model can be used for the investigation of conditions for maximum extraction of energy by varying the mass of the device and its damping.

5. Wave flume testing of the OWEC

The wave flume that was employed for tank testing is located in Springfield, OR and is 7 ft deep, 30 ft wide and 110 ft long and tapers to a typical beach. There are two sets of hydraulically driven wave makers that are activated in sequence to create irregular waves of approximately 4 ft in height and with approximately 4 s dominant periods. The OWEC was tested in irregular waves in order to prove the design concept. Fig. 14 shows the device under testing in the Springfield wave flume. This configuration of the device is shown in Fig. 2 with a rigid shaft between the inner module and the mooring plate. The shaft is also equipped with a swivel joint that allows motion in six degrees of freedom. However, the threaded studs of the swivel joint can be adjusted to provide a stiff rigid member.

The oscilloscope capture in Fig. 15 shows the no-load voltage of the electric generator during the up- and down-

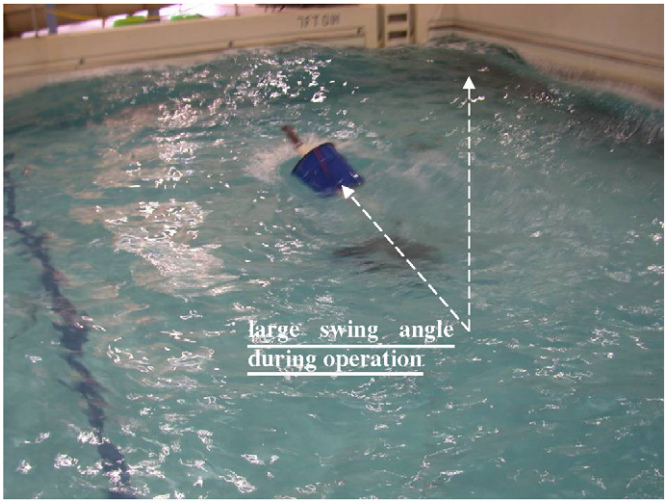

Fig. 14. OWEC with CFTS during wave tank testing.

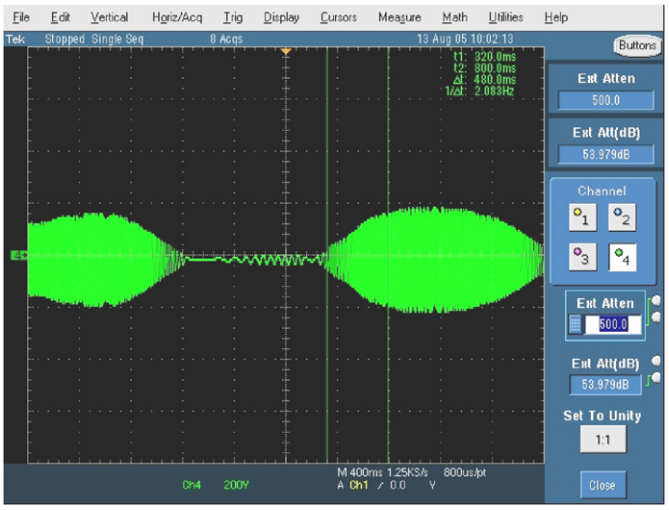

Fig. 15. Generator no-load voltage during wave tank testing.

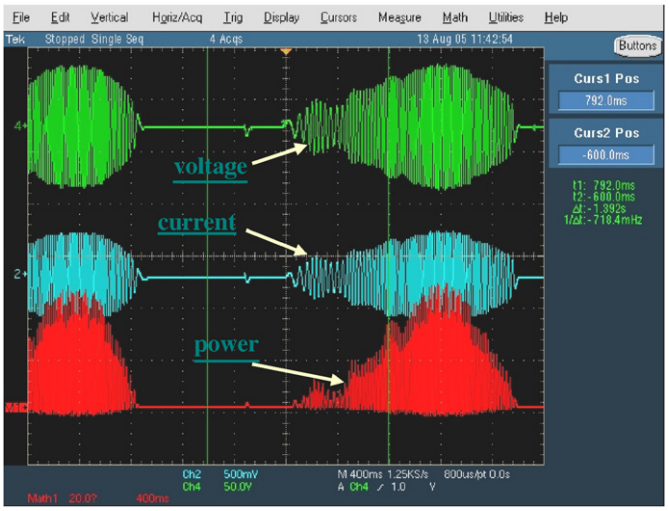

Fig. 16. Generator voltage, current and power during wave tank testing.

stroke portions of the wave cycle. Because of the uni-directional clutch, the generator free wheels on the down stroke and no voltage is generated. Fig. 16 shows a typical oscilloscope capture of the output of the OWEC operating into a 75 Ω load, showing waveforms for the voltage (green), current (blue) and power (red). The peak output power under load was about 69 W. Although it fits into the inner module nicely as required, the generator's synchronous reactance is very high and the voltage drop across it was also high. It is anticipated that with a generator of relatively lower impedance, the output power will greatly improve. Also, the large swing angles (see Fig. 14) experienced during the operation significantly reduced the amount of travel available to the buoy on both upstroke and down stroke. The swing angle can be modified by adjusting the swivel joint to other positions but this was not fully investigated at that stage of testing.

Table 3 shows additional test results under different generator loading conditions. Considering that this is a

Author's personal copy

Table 3
Wave flume test results of OWEC

Load resistance (Ω)	Voltage, V_p (V)	Current, I_p (A)	Power, W_p (W)
20	16	0.5	6
30	35	0.7	18.4
50	52	0.6	23.4
75	65	0.6	29.3

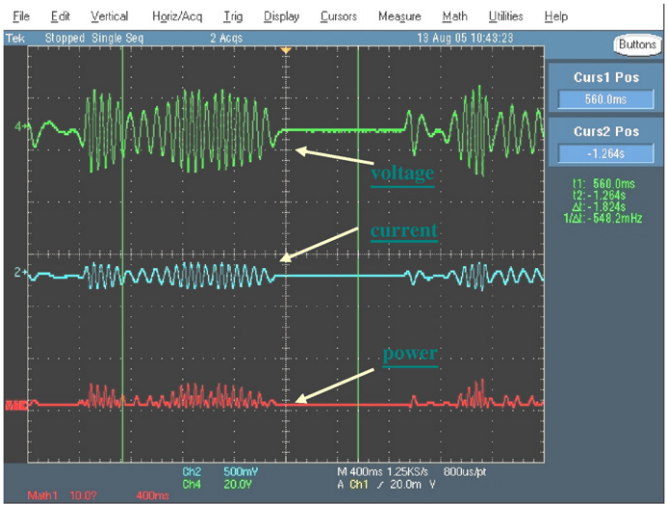

Fig. 17. Generator voltage, current and power showing irregular motion of the shaft system caused by irregular wave excitation.

scaled model of the device, the power output obtained is reasonably significant. Using Froude scaling laws, it was estimated that a full-scale prototype of this device would be able to produce a nominal power output of about 30 kW in typical Oregon seas [12]. This corresponds to a device diameter of about 6 m and a length of about 10 m.

Fig. 17 shows a typical waveform showing the irregular motion of the shaft system due to the irregular wave excitation. The irregular strokes that resulted from these wave conditions sometimes tend to stall the shaft rotation on the upstroke cycles where it should be spinning. The stall behavior is a direct consequence of the friction performance of the ball screw. It is proposed that this can be overcome with a good dynamic control system that takes into account the effects of irregular waves on friction performance and, in general, the friction behavior of the ball screw. A friction model of the ball screw has been reported in literature and the control techniques that are required are already being pursued by other researchers [13].

Additional testing was carried out in the O.H. Hinsdale Wave Research Laboratory, where the rigid mooring configuration was changed to a slack-mooring configuration with the help of a drag plate connected to the inner

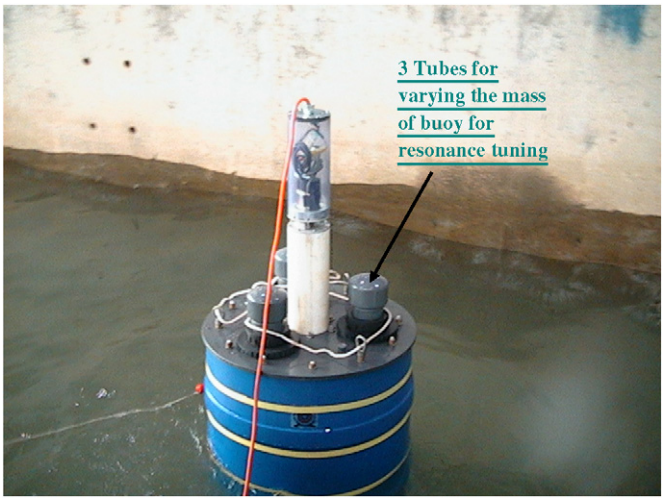

Fig. 18. Slack-moored OWEC under test in O.H. Hinsdale Wave Research Lab.

module. Provisions were also made for varying the total mass of the buoy by inserting weights into three equilaterally placed pvc tubes in the float. Fig. 18 shows the new configuration in the long wave flume of the O.H. Hinsdale wave research laboratory. Further testing of this configuration is planned, including on a comprehensive linear test bed and the details of this design configuration and further test results will be documented in a subsequent paper.

Future work on the slack moored configuration of the device shown in Fig. 18 includes investigations into different drag plate designs, with a view to understanding their effect on power capture.

6. Conclusion

A CFTS has been designed to transfer thrust from an outer cylindrical back iron to an inner piston. The device enabled the design of a new OWEC in which an outer float was coupled to a PTO mechanism, comprising the piston and a ball screw shaft with a mounted rotary generator. Because the coupling is through magnetic means, the inner module containing the piston and the generator was completely sealed. Several design options of the final prototype of the CFTS have been compared through finite element simulations and experimental testing, with good agreement. The optimal design of the system chosen was based on the criterion of maximum peak axial thrust.

Based on the chosen configuration, a new OWEC was designed and successfully tested in irregular waves in a flume. The device consists of an outer float of diameter 0.6 m and of length 0.6 m. A design configuration of this device with a drag plate and provisions for varying the mass of buoy was tested in the O.H. Hinsdale Wave Research Laboratory for performance. Further tests,

Author's personal copy

including on a comprehensive linear test bed, will be conducted and documented in a subsequent paper.

Acknowledgment

While this paper was being reviewed for publication, Dr. Alan K. Wallace passed away after a brief illness on June 7, 2006. The authors dedicate this paper to the memory of their friend, colleague and mentor.

Appendix A

Appendix A.1

See Table A.1

Table A.1
Generator parameters

Manufacturer	Ametek
Type	BLDC
Rated voltage (V)	270
Phase	3
RPM	12 000
R_s, X_s (Ω)	0.43, 0.19

Appendix A.2

Dimensions (mm) of piston/cylinder.

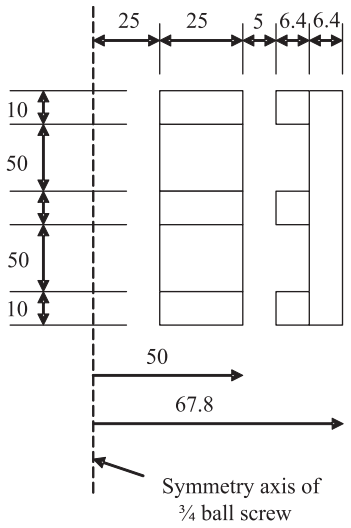

References

[1] Rhinefrank K, Agamloh EB, von Jouanne A, Wallace AK, Prudell J, Kimble K, et al. A novel ocean energy permanent magnet linear generator buoy. Renew Energy 2006;31(9):1279–98.
[2] Mueller MA. Electrical generators for direct drive wave energy converters. Proc IEE Gen Trans Distr 2002;149(4).
[3] Wang J, Jewell GW, Howe D. A general framework for the analysis and design of tubular linear permanent magnet machines. IEEE Trans Magn 1999;35.
[4] Wang J, Howe D. Analysis of axially magnetized, iron-cored tubular permanent magnet machines. IEE Proc Electr Power App 2004;151(#2).
[5] Faiz J, Finch JW. Aspects of design optimization for switched reluctance motors. IEEE Trans Energy Convers 1993;8(4).
[6] Hornreich RM, Shtrikman S. Optimal design of synchronous torque couplers. IEEE Trans Magn 1978;MAG-14(5).
[7] Yonnet JP, Hemmerlin S, Rulliere E, Lemarquand G. Analytical calculation of permanent magnet couplings. IEEE Trans Magn 1993;29(6).
[8] David Meeker, FEMM 〈http://femm.foster-miller.net〉.
[9] McCormick ME. Ocean engineering wave mechanics. Wiley; 1973.
[10] Mei CC. Power extraction from water waves. J Ship Res 1976;20(2).
[11] Bertreaux HO. Buoy Engineering. Wiley; 1976.
[12] Emmanuel B. Agamloh, A direct-drive wave energy converter with contact-less force transmission system, PhD dissertation, Oregon State University, Corvallis, 2005.
[13] Jang MJ, Lin KC, Chen CL. Modeling and position control of a ball screw stage. In: Proceedings of the IEEE international conference on networking, sensing and control, Taipei, Taiwan, March 2004.